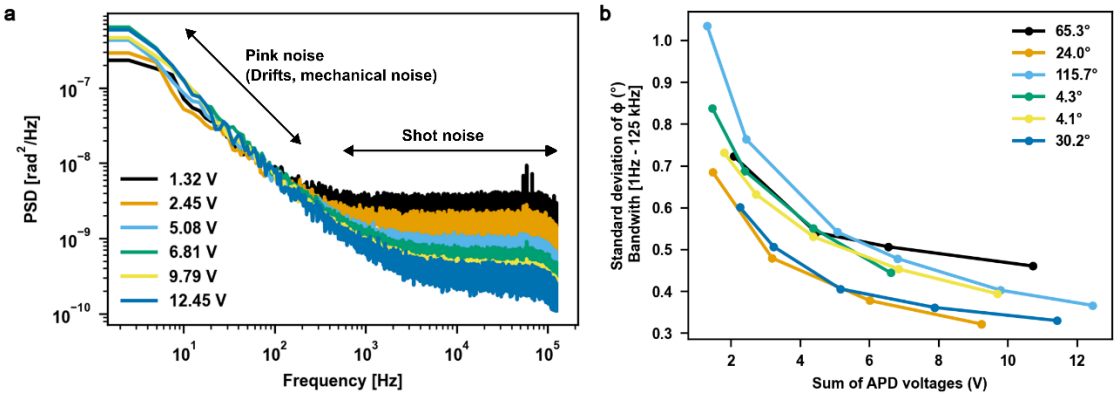

Extended Data Figure 1: Measurement noise of the orientation of five stuck rods on a glass surface. **a.** Power spectral density of the angular signal of the stuck rod corresponding to the integrated signal in green on the left. The flat portion at high frequencies corresponds to the shot noise and depends on the light intensity received in the APD. The left portion, with exponent -1, is pink noise due to various drifts in the optical system. **b.** Integrated noise in degrees as a function of the captured light intensity, modulated by changing the laser power. The labels indicate the average orientation ϕ of the rod.

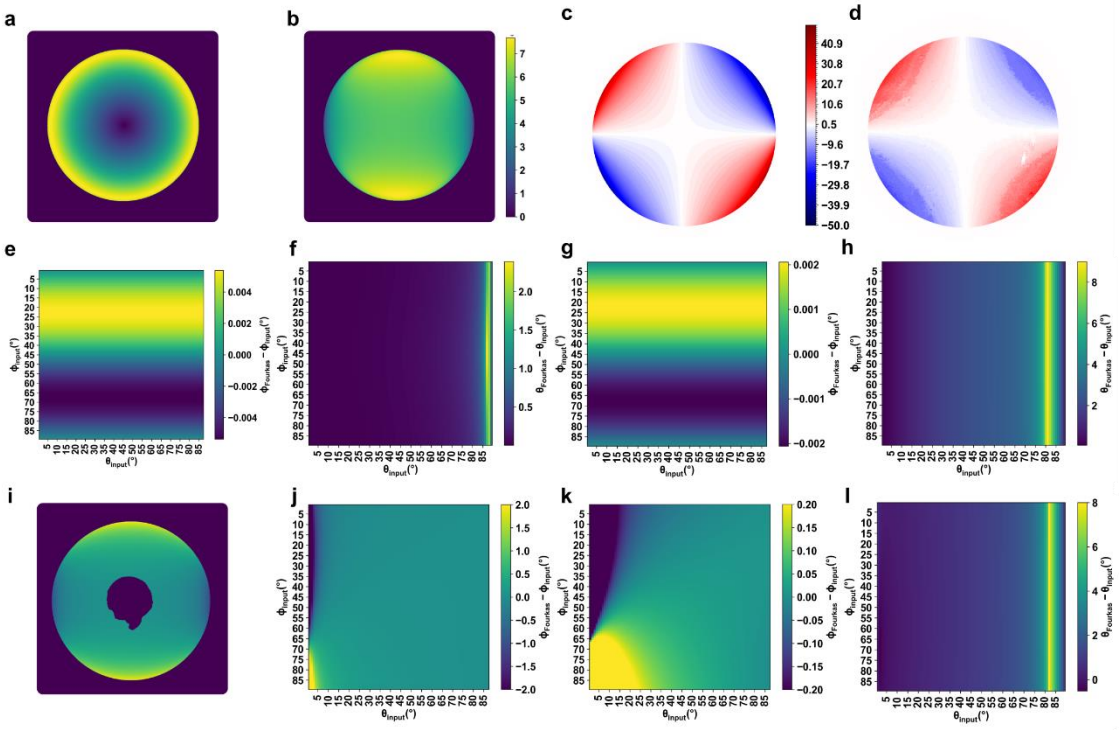

Extended Data Figure 2: Simulation of the radiation of a dipole in focus as observed in the back-focal plane. a-b. Intensity profile in the back focal plane (arbitrary units). **a**: θ = 0°, **b:** θ = 90°. **c**: Simulated orientation of the electric field as a function of the position in the back focal plane (in degrees). **d.** Polarization direction as measured in the back focal plane of the objective by putting a linear polarization filter in focus. **e.** Difference between ϕ used as input in the simulation and the retrieved

angles after applying Fourkas formula to the integrated intensities in the back focal plane. As a function of ϕ and θ used as simulation input. **f.** Same as e. but for θ. **g-h.** Same as e-f but adding in the simulation the effect of refraction on polarization at the water/glass interface. **i.** Same as b. but superimposing the hole in the mirror to the BFP. **j-k-l**. Same as g-h in the case of a hole in the back focal plane. **j** and **k** only differ by the angle range used in the colour bar. Deviations are less than 1 degree except in θ very near θ= 90° (horizontal rods) and in ϕ very near θ= 0° (vertical rods).

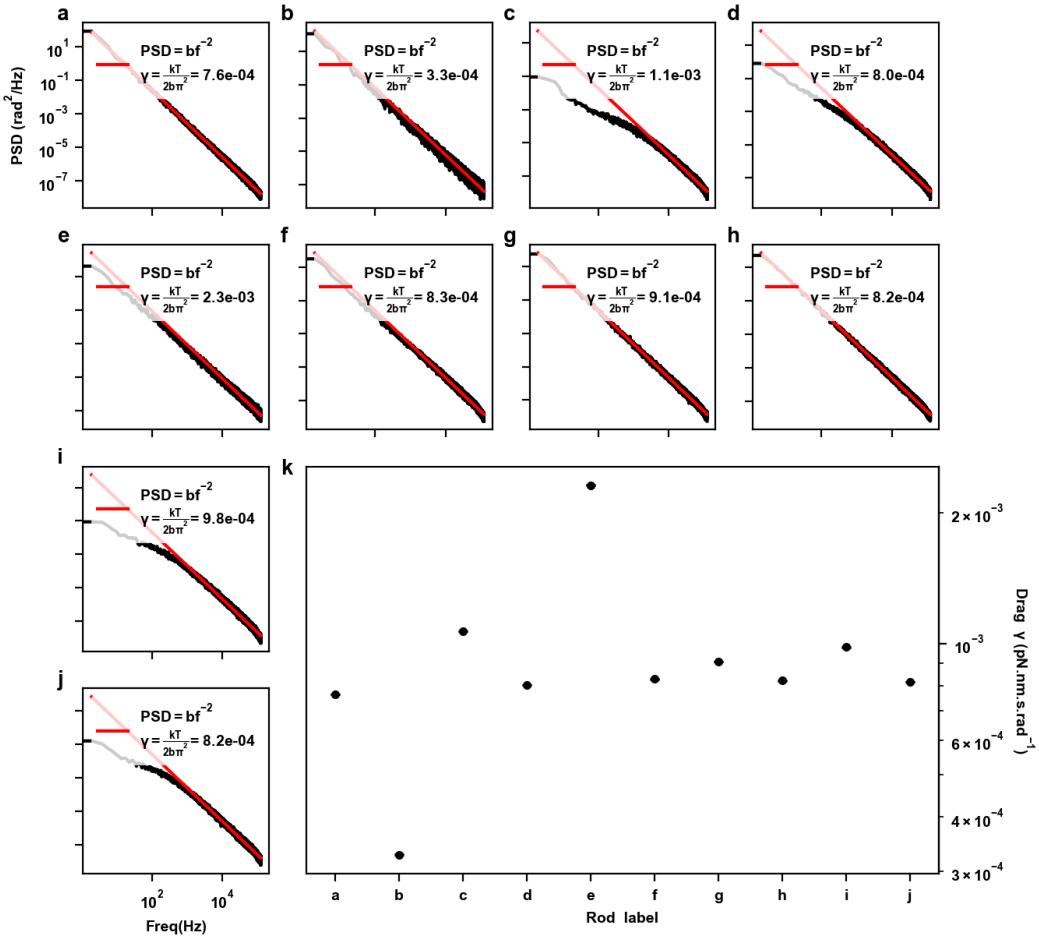

Extended Data Figure 3: Power spectral density and inferred rotational drag of 10 loosely surface-attached rotating rods. a–j: Power spectral density of angular motion for each rod, with $b \times f^2$ fits shown at high frequencies. Axis ticks are consistent across all panels and labelled in a and j. **k**: Summary of inferred rotational drag coefficients.

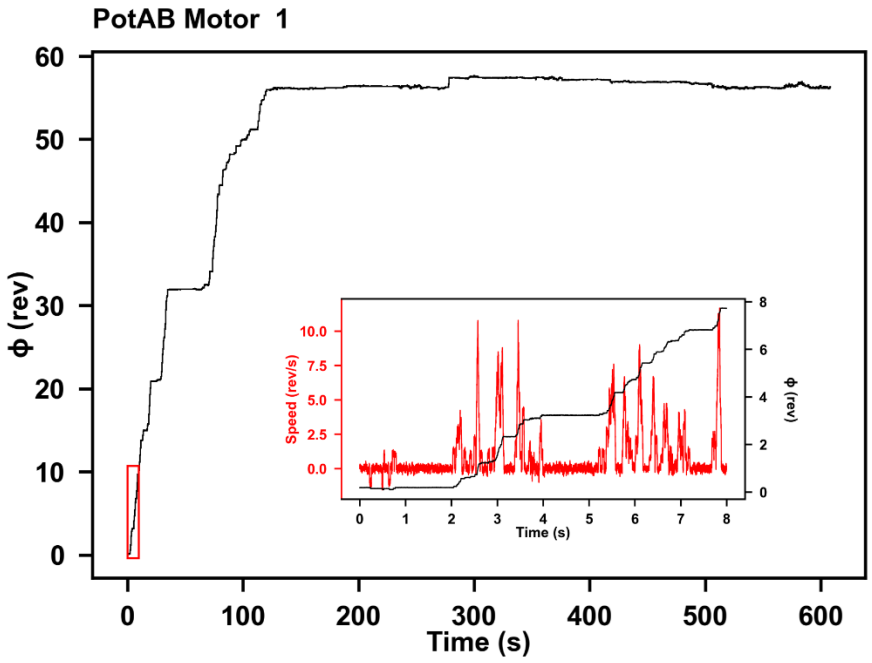

Extended Data Figure 4: Angular trajectory of PotAB Motor 1 following buffer exchange (~0 mM NaCl). Inset: Zoomed-in view showing angular position (black) and speed (red), with speed derived as the time derivative of angle and smoothed over a 40-ms running window.

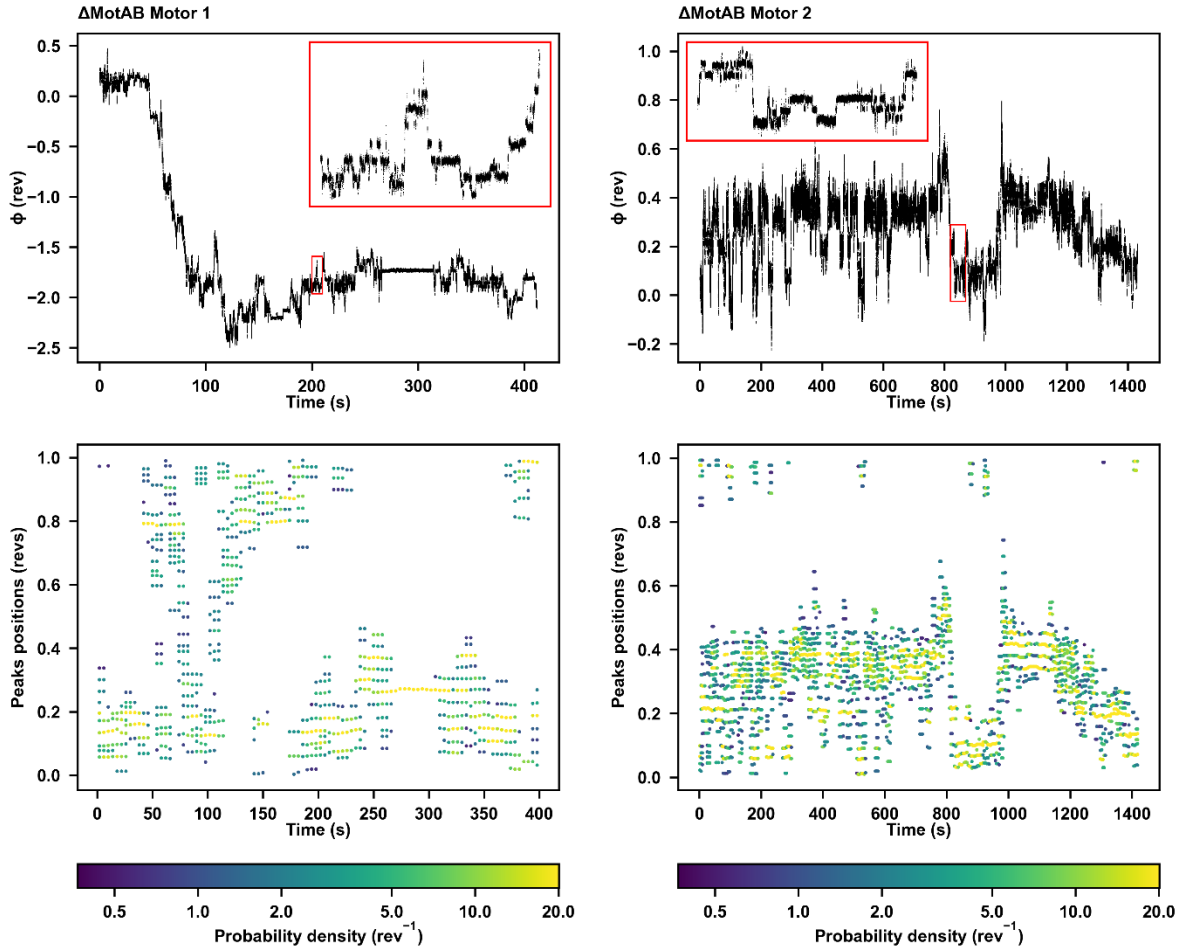

Extended Data Figure 5: Diffusion dynamics of MotAB Motors 1 and 2. Top: Angle versus time trace of a passively rotating motor. **Bottom:** Evolution of peak positions in angular histograms computed over overlapping 10 s windows, shifted every 4 s. Colour bar indicates the probability density (rev^{-1}) at each peak. Lower peaks (dark blue) are more error-prone. See also supplementary videos S4, S5.

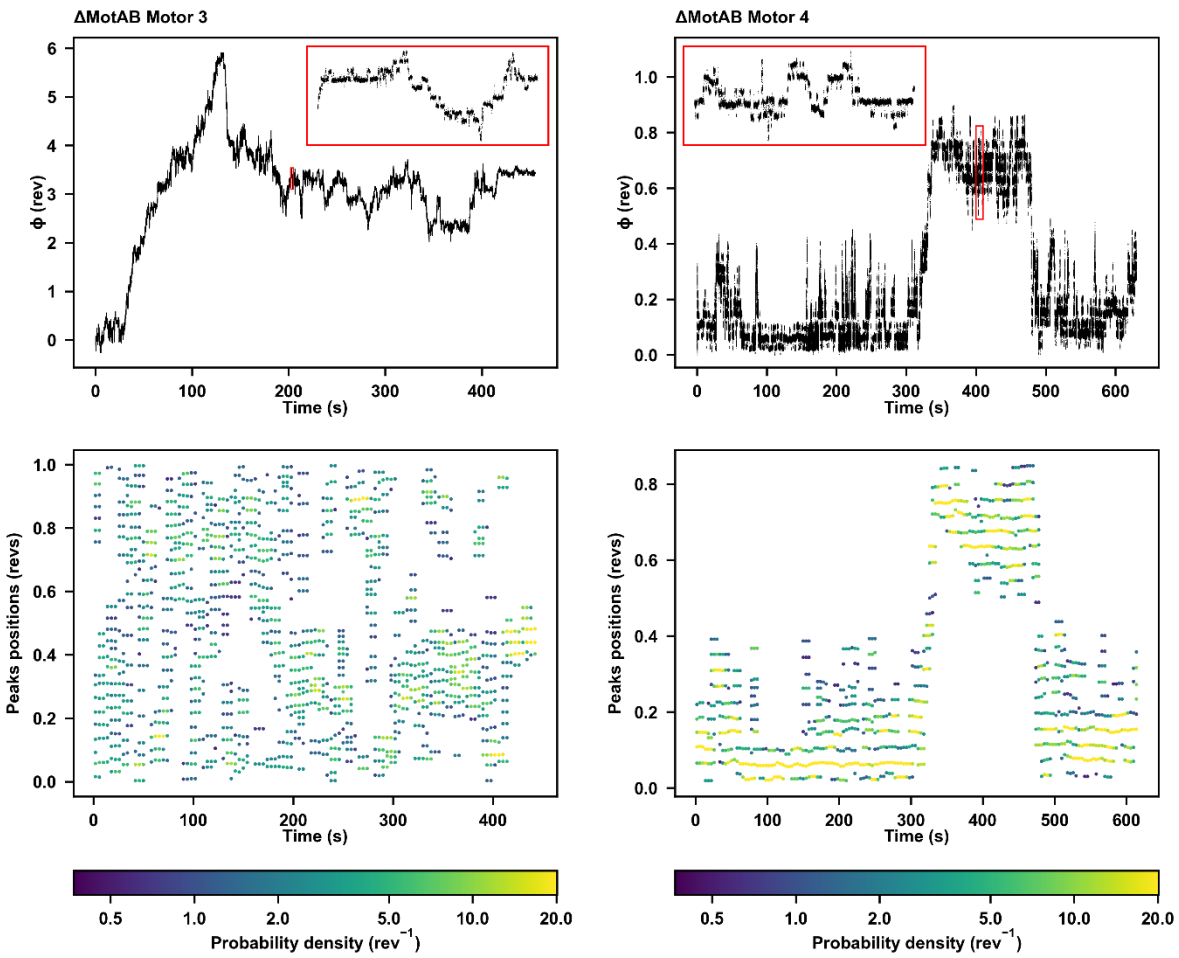

Extended Data Figure 6: Diffusion dynamics of MotAB Motors 3 and 4. Top: Angle versus time trace of a passively rotating motor. **Bottom:** Evolution of peak positions in angular histograms computed over overlapping 10 s windows, shifted every 4 s. Colour bar indicates the probability density (rev^{-1}) at each peak. Lower peaks (dark blue) are more error-prone. See also supplementary videos S6, S7.

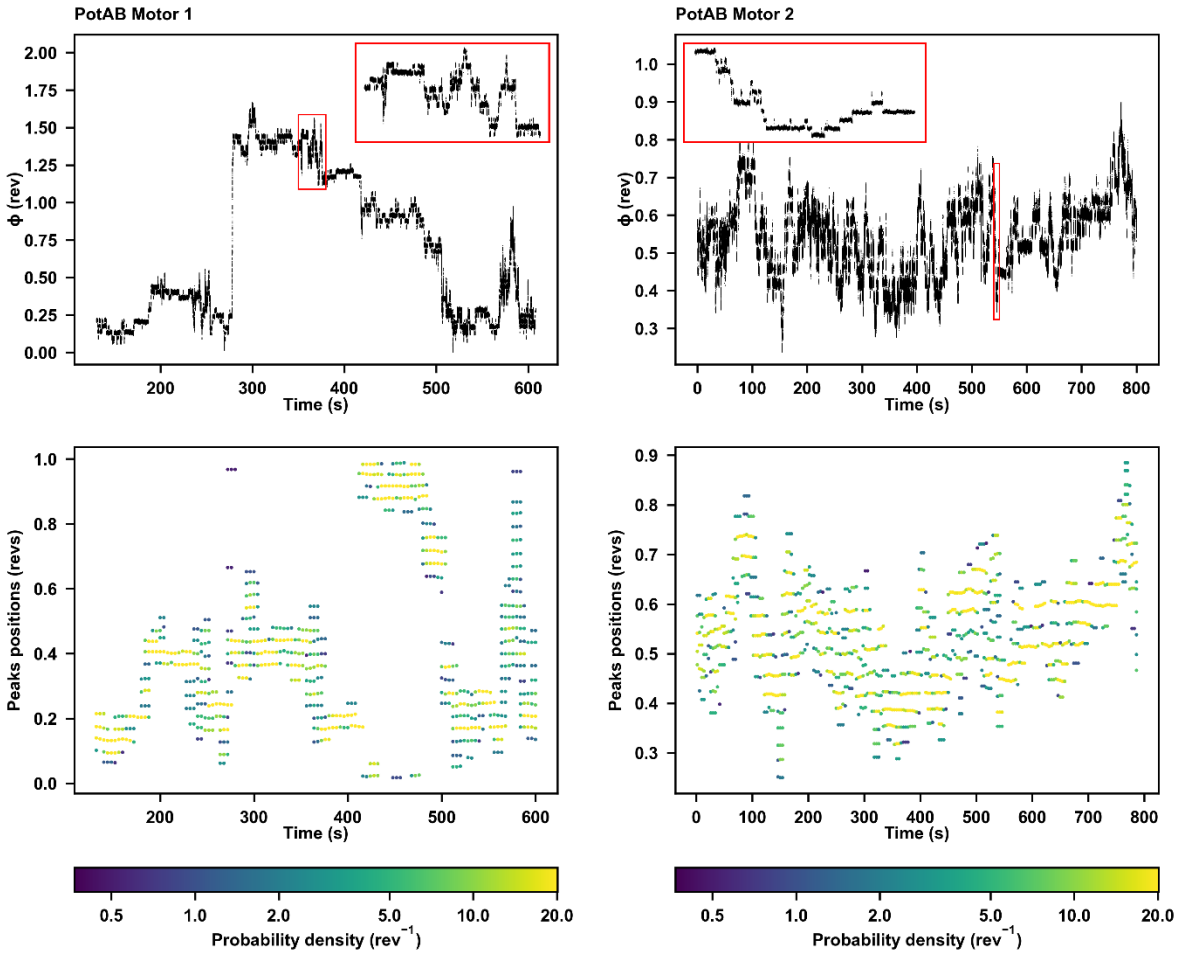

Extended Data Figure 7: Diffusion dynamics of PotAB Motors 1 and 2. Top: Angle versus time trace of a passively rotating motor. **Bottom:** Evolution of peak positions in angular histograms computed over overlapping 10 s windows, shifted every 4 s. Colour bar indicates the probability density (rev^{-1}) at each peak. Lower peaks (dark blue) are more error-prone. See also supplementary videos S1, S2.

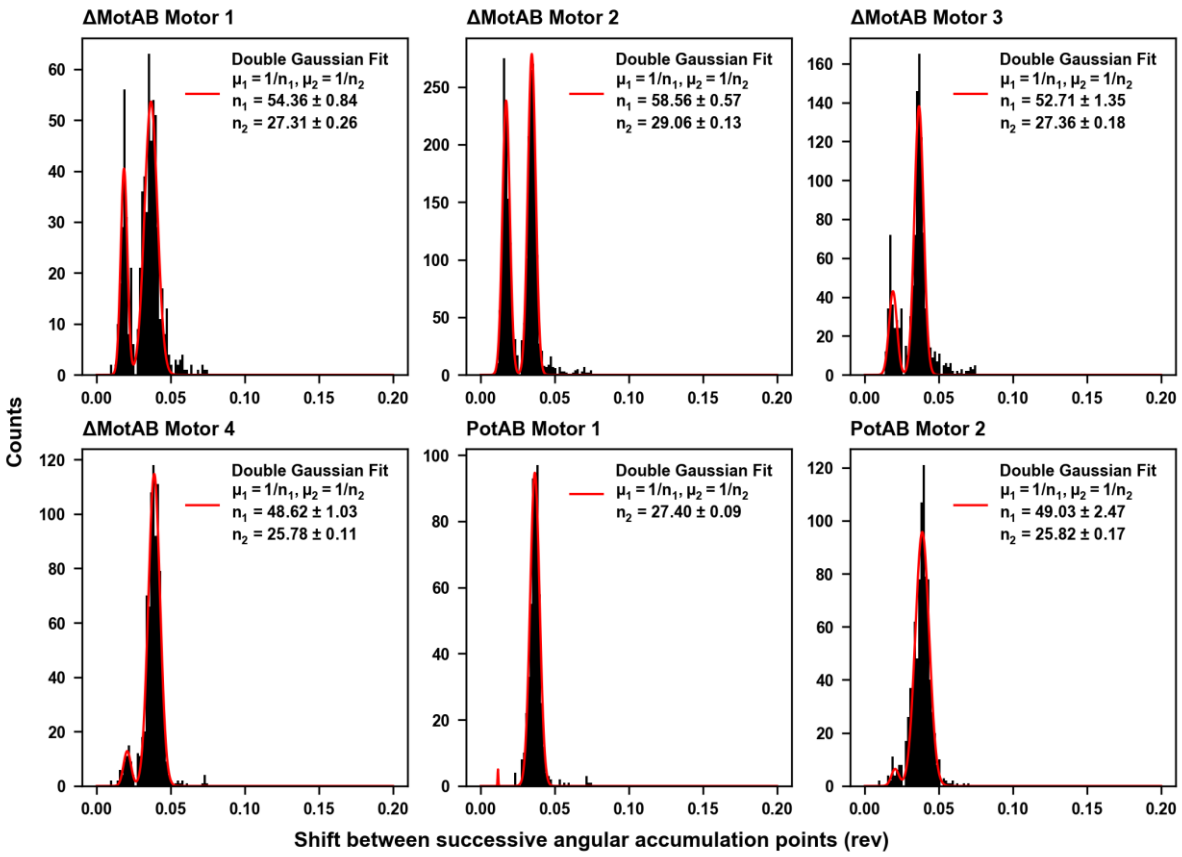

Extended Data Figure 8: Distribution of angular shifts between successive accumulation peaks for individual motors. The histograms show the distribution of angular displacements between consecutive peak positions identified in angular histograms (see Extended Data Fig. 5-7). In addition to the dominant peak separation close to 1/26 rev, several motors show a peak separation half this size, corresponding to smaller steps which are ignored by the step-finding analysis. Each panel corresponds to a single motor. Red lines represent double Gaussian fits with inverse peak positions ($\mu_1 = 1/n_1$, $\mu_2 = 1/n_2$) and associated fitting parameters.

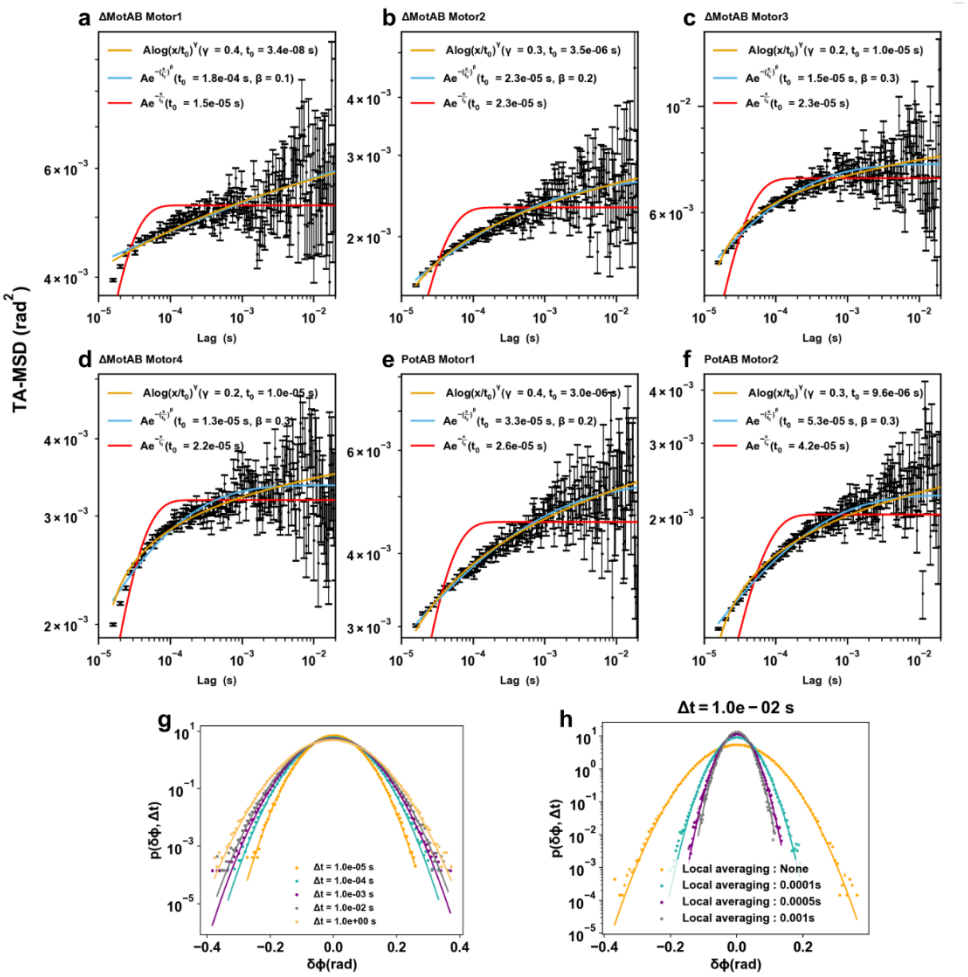

Extended Data Figure 9: Angular fluctuation analysis during 1-second dwells. a–f: Time-averaged mean-square displacement (TA-MSD) during individual 1-second dwells (no steps), one per motor, fitted with exponential, stretched-exponential, and logarithmic relaxation. Error bars correspond to $\sigma/\sqrt{N_s}$, where σ is the standard deviation of the N_s independent MSD values for each lag. **g:** Probability distributions $p(\delta\phi, \Delta t)$ of angular displacements at increasing lag times Δt, showing Gaussian behavior across timescales (from the dwell analysed in e.). **h:** Angular displacement distributions at fixed lag time (Δt =0.01) under different levels of local averaging to remove high-frequency noise; Gaussian nature is preserved.

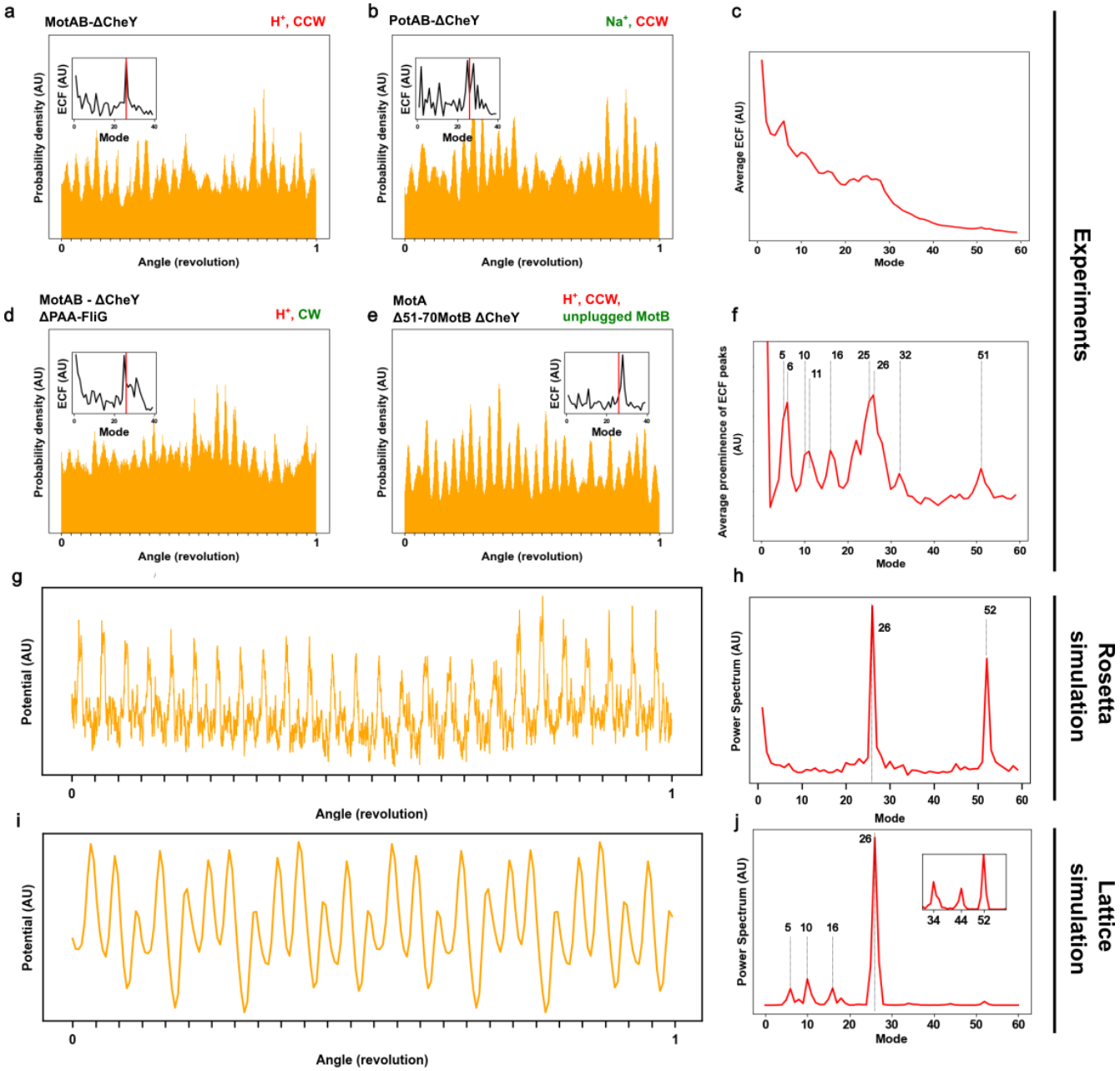

Extended Data Figure 10: a-d. Histograms of the rotation angle ϕ averaged over 10s for four different motors of different strains. The variability of the histograms cannot be attributed to a particular mutant as within one strain they display similar variabilities. Insets: empirical characteristic function (ECF) showing the main periodicities in dwell angle. The red line shows the mode 26. CW: clockwise. CCW: counterclockwise. **e.** Average ECF over all non-overlapping 0.4 s windows (10^5 data points) over 18 motors from different strains. The variation of background in the ECF from file to file smoothens the peaks. **f.** Average prominence of each ECF mode over the same windows as in e. We define the prominence as the power of a particular mode divided by the minimum power over that mode and its four nearest neighbours. **g.** Energy landscape of the LP-ring / rod interface calculated via Rosetta using the cryo-EM structure from Salmonella (PDB 7CGO, see Methods for details). **h.** Amplitude of the Fourier transform of G. **i.** Energy landscape simulated using a simplified lattice-model of the cryo-EM structure (Supplementary Note S7). **j.** Amplitude of the Fourier transform of i.